CHEMISTRY OF MATERIALS

Article

pubs.acs.org/cm

Nanocrystalline MOFs Embedded in the Crystals of Other MOFs and Their Multifunctional Performance for Molecular Encapsulation and Energy-Carrier Storage

Kyung Min Choi,† Jung Hyo Park,† and Jeung Ku Kang*

Graduate School of Energy, Environment, Water, and Sustainability (EEWS) and Department of Materials Science and Engineering, Korea Advanced Institute of Science and Technology (KAIST), Daejeon 305-701, Republic of Korea

Supporting Information

ABSTRACT: A metal−organic framework (MOF) with a specific construction and pores was demonstrated to have many advanced properties, but still limited to having unique aspects arising from the combination of different MOFs in a single body. Here, we report a facile method to produce MOF-5 crystals with nanocrystalline HKUST-1 (nHKUST-1) embedded into them in what is termed the "nHKUST-1⊂MOF-5" structure. The results show that the nHKUST-1⊂MOF-5 structure is capable of molecular encapsulation by trapping dye molecules in nHKUST-1 particles and embedding them in MOF-5 crystals. Moreover, the gravimetric uptake capacity of nHKUST-1⊂MOF-5 for methane (CH_4) was found to be enhanced as compared to that of MOF-5 or nHKUST-1 alone such that the nHKUST-1⊂MOF-5 structure exhibits a volumetric capacity of 250% for fuel storage deliverable by the CNG tank at room temperature and 80 bar. Furthermore, it showed robust capacity retention for reversible CH_4 uptake cycles at room temperature.

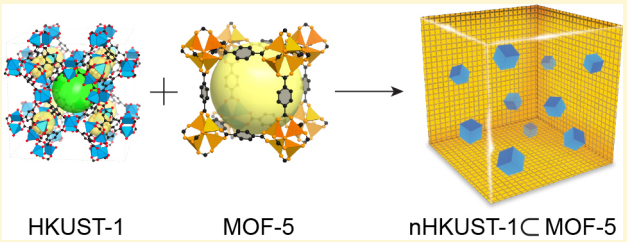

INTRODUCTION

The design and synthesis of a crystalline nanoporous framework usually originate from a combination of single constituents into an underlying matrix to form its own properties.[1−4] For example, a metal−organic framework (MOF) uses a specific organic linker and the secondary building unit (SBU) of a metal−oxide constituent typically to realize its unique crystalline and porous structure,[5,6] whereas modification by a different organic linker or an inorganic moiety can tune the underlying structure to have various properties.[7−10] This hierarchy allows facile control of the structure and its properties, but some challenges remain when one pursues the goal of developing a simple means of creating new aspects arising from a combination of completely different MOFs in a single body.

Here, we report a new method in which completely different MOFs are combined into a single crystalline particle. This method can introduce many opportunities to form a series of heterogeneities in MOFs by embedding other nanocrystals of MOFs (nMOFs) with special constructions and micropores, as illustrated in Figure 1. This unique construct is expected to generate new interfaces of two MOFs, thus providing unusual properties that differ from those observed using only a single type of MOF. In this study, we demonstrate how to produce crystals of MOF-5 [$Zn_4O(BDC)_3$ (BDC = 1,4-benzenedicarboxylate)],[11] which embed nanocrystalline HKUST-1 [nHKUST-1, $Cu_3(BTC)_2$ (BTC = 1,3,5-benzenetricarboxylate)],[12] known as nHKUST-1⊂MOF-5, hereafter. Moreover, we find that this construct is able to encapsulate guest molecules such as molecular dyes in nHKUST-1, with these molecules subsequently embedded into MOF-5 crystals. In addition, nHKUST-1⊂MOF-5 shows a high CH_4 uptake capacity (197 mg/g, 80 bar) at room temperature, corresponding to 250% of the deliverable volumetric capacity by a commercially available CNG (compressed natural gas) tank. It is notable that the methane (CH_4) has a high specific energy density (15 400 Wh/kg).

Previous studies have reported synthetic approaches to coat metal nanoparticles with organic/inorganic materials[13−17] and to disperse heterogeneous atoms in nanomaterials,[18−21] but none of these nanomaterials are porous. Some efforts have been made to combine MOFs with metal nanoparticles by impregnation followed by reduction,[22,23] coating,[24,25] and embedment,[26,27] while core/shell types of MOFs have been made using two different functional linkers but with the same SBUs.[28,29] However, no study has shown nanocrystalline MOFs embedded in other MOF crystals having completely different linkers and SBUs.

EXPERIMENTAL SECTION

Synthesis of nHKUST-1. Copper acetate monohydrate (215 mg) and 1,3,5-tricarboxylic acid (125 mg) were dissolved in 75 mL of a 1:1:1 mixture of DMF/EtOH/H_2O in a round-bottomed flask. The mixture was then stirred for 1 h at room temperature. The product was

Received: May 13, 2015
Revised: June 19, 2015
Published: June 23, 2015

DOI: 10.1021/acs.chemmater.5b01786
Chem. Mater. 2015, 27, 5088−5093

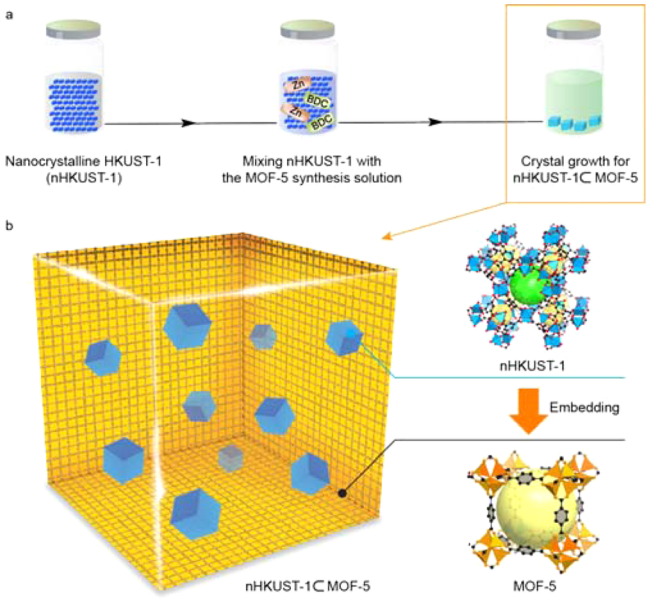

Figure 1. (a) Schematic procedures for creating the nHKUST-1⊂MOF-5 structure, and (b) schematic diagram of the nHKUST-1⊂MOF-5 structure.

collected by a centrifuge (9000 rpm for 10 min), washed two times with DMF, and immersed in EtOH for 3 days. The solvent was exchanged for fresh solvent three times. Finally, the nHKUST-1 was activated to remove the solvent under a vacuum for 24 h at 100 °C.

Synthesis of MOF-5. Zinc nitrate tetrahydrate (392 mg) and terephthalic acid (83 mg) were first dissolved in DEF (5 mL) in a 20 mL vial. The tightly capped vial was placed on a hot plate at 150 °C for 3 h to yield clear crystals. After being cooled, the yellow solution was decanted and the crystals were washed with 20 mL of DMF three times. The product was then immersed in chloroform for 3 days, during which time the activation solvent was decanted and freshly replenished three times. Finally, the MOF-5 was activated to remove the solvent under a vacuum for 24 h at 120 °C.

Synthesis of nHKUST-1⊂MOF-5. Zinc nitrate tetrahydrate (1764 mg) and terephthalic acid (375 mg) were dissolved in DEF (16 mL) in a 30 mL vial. nHKUST-1 fabricated by the above-mentioned method was then dispersed in DEF (20 mL). Subsequently, the nHKUST-1 solution (4 mL) was put into a mixed solution of zinc nitrate tetrahydrate and terephthalic acid. The color of the solution was changed from blurry blue to transparent bluish by sonication for 20 min. The vial was then put into an oven at 110 °C for 7 h for the growth of the crystals. The products were washed with DMF two times and immersed in chloroform for 3 days, exchanging the solvent three times. Finally, the nHKUST-1⊂MOF-5 was activated to remove the solvent under a vacuum for 24 h at 120 °C.

Characterization of the Materials. The resulting products were characterized by experiments using optical microscopy, PXRD, transmission electron microscopy (TEM), high-angle annular dark-field (HAADF), scanning transmission electron microscopy (STEM), SEM, nitrogen gas adsorption, inductively coupled plasma atomic emission spectroscopy (ICP-AES), and NMR measurements, which demonstrated their crystallinity, permanent porosity, embedment, and the composition of nHKUST-1 nanocrystals in the MOF-5. Full characterization details are provided in the Supporting Information.

RESULTS AND DISCUSSION

HKUST-1 and MOF-5 were chosen as examples because both are typical MOFs and are composed of completely different structures, space groups, linkers, and SBUs. nHKUST-1 was prepared using a mixture of $Cu(OAc)_2{\cdot}H_2O$ and 1,3,5-benzenetricarboxylic acid and a 1:1:1 mixture of *N,N*-dimethylformamide(DMF)/EtOH/H_2O at room temperature, which led to the creation of nanocrystals (ca. 100 nm) of HKUST-1 after washing with DMF and EtOH and drying under a vacuum. The crystallinity of nHKUST-1 was examined by the PXRD (powder X-ray diffraction) method, which gave sharp diffraction peaks matching those of the simulated patterns (Figure 2a). The permanent porosity was also confirmed by

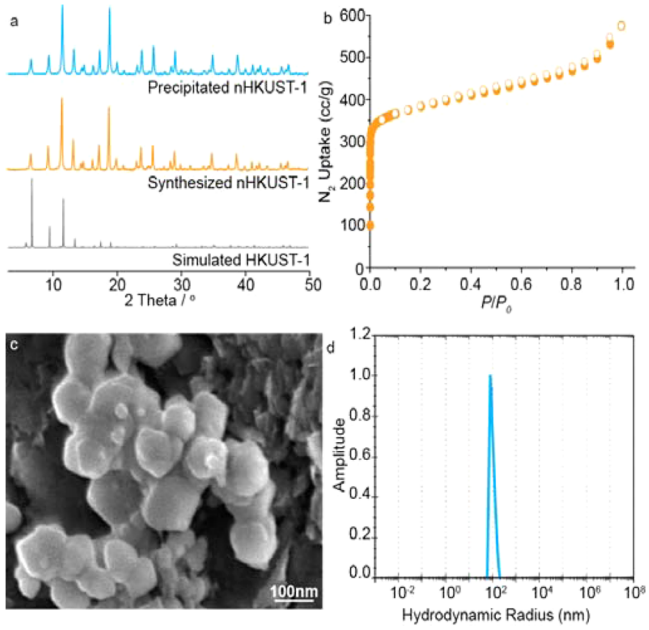

Figure 2. Structural analyses of the nHKUST-1 samples: (a) X-ray diffraction patterns of the crystalline powder of the precipitated nHKUST-1, the synthesized nHKUST-1, and the simulated HKUST-1. (b) N_2 gas-adsorption isotherm of nHKUST-1. (c) SEM image of nHKUST-1. (d) Dynamic light-scattering (DLS) analysis of nHKUST-1.

measuring the nitrogen gas sorption isotherm. It showed a shape similar to that observed for this MOF (Figure 2b) and gave a BET surface area of 1470 m^2/g. The SEM image of nHKUST-1 showed an average crystal size of 100 nm (Figure 2c).

The dried nHKUST-1 was then placed in a MOF-5 preparation solution with $Zn(NO_3)_2{\cdot}6H_2O$ and 1,4-benzenedicarboxylic acid in *N,N*-diethylformamide (DEF). When nHKUST-1 was initially mixed with the chemicals in DEF, the mixed solution was opaque due to the suspension of the nHKUST-1 particles (Figure 1a). After 10 min of ultrasonication, the solution became transparent blue and no suspensions were observed. To show that nHKUST-1 particles were not dissolved out but were solvated in the solution, we measured the particle sizes by means of dynamic light-scattering (DLS). Figure 2d demonstrates that there were particles about 100 nm in size, indicating that the particles were not dissociated. The particles in the solution then were precipitated out by adding an excess amount of acetone and washing with DMF, and then measured with the PXRD method. We found that the PXRD results of the particles matched those of the nHKUST-1 structure (Figure 2a), thus supporting the finding that the nHKUST-1 particles were not dissociated but remained as solvated nanocrystalline particles in the MOF-5 preparation solution. Next, this solution was heated

DOI: 10.1021/acs.chemmater.5b01786
Chem. Mater. 2015, 27, 5088−5093

in an oven at 110 °C, which induced the formation of nHKUST-1⊂MOF-5 (Figure 1b).

The crystallinity of the nHKUST-1⊂MOF-5 structure was proven from the sharp diffraction lines of its PXRD patterns (Figure 3a). The coincidence of diffraction lines with those of the MOF-5 indicates that its overall structure is identical to that of the MOF-5, but the diffraction lines for nHKUST-1 particles were not observed in the pristine form of the nHKUST-1⊂MOF-5 sample. When the samples were ground into fine powers, the diffraction lines for the nHKUST-1 particles appeared (Figure 3a). These results support the contention that the nHKUST-1 nanocrystals are located in the interior rather than on the surface of the MOF-5. In addition, the permanent porosity of the nHKUST-1⊂MOF-5 sample was determined through nitrogen (N_2) gas-adsorption isotherm measurements, which exhibited Type I behavior similar to that observed in the MOF-5 (Figure 3b). However, its pore-size distribution showed two different pores: one (6 Å) from nHKUST-1 and the other (9 Å) from MOF-5, as shown in Figure S1 of the Supporting Information. The Langmuir surface area of nHKUST-1⊂MOF-5 was 3400 m^2/g.

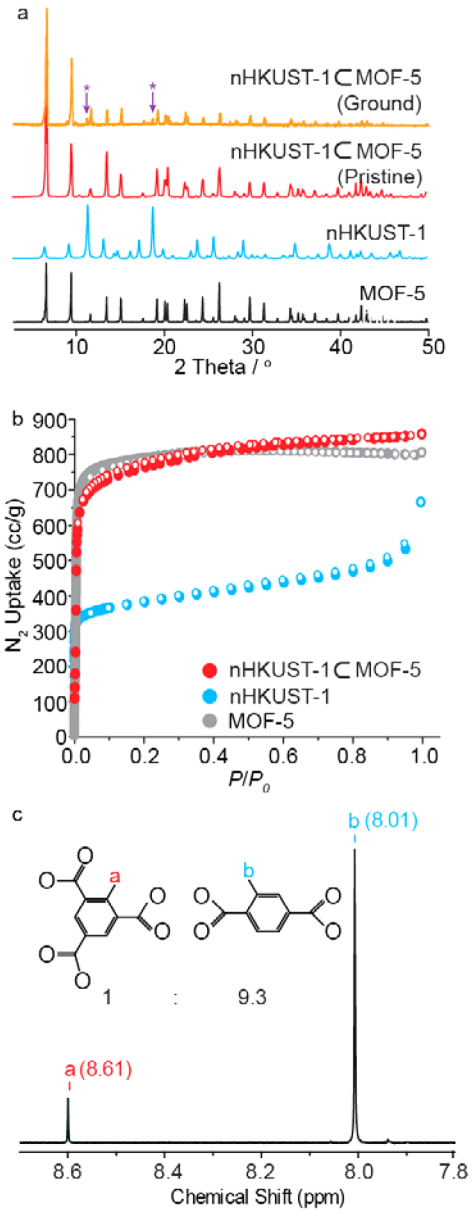

Figure 3. Structural analyses of nHKUST-1⊂MOF-5 samples: (a) X-ray diffraction patterns of crystalline powders of the MOF-5, nHKUST-1, and nHKUST-1⊂MOF-5 samples. (b) Nitrogen gas-adsorption isotherms of the MOF-5, nHKUST-1, and nHKUST-1⊂MOF-5 samples. (c) ^{1}H NMR spectra of the digested nHKUST-1⊂MOF-5 sample.

Furthermore, the chemical composition of the sample was obtained from the ^{1}H NMR spectra of its HCl-digested solution (Figure 3c) and from an ICP-AES analysis. The ^{1}H NMR peaks corresponding to the linkers of HKUST-1 (H_2BTC) and MOF-5 (H_2BDC) were used to determine the ratio of nHKUST-1 in nHKUST-1⊂MOF-5. The molecular ratio (H_2BTC:H_2BDC = 1:9.3) of the linkers indicated that the 11 wt % of nHKUST-1 is embedded into the nHKUST-1⊂MOF-5 sample. Also, the ICP-AES data for the metals of nHKUST-1 (Cu, 10 wt %) and MOF-5 (Zn, 90 wt %) indicate that the ratio of nHKUST-1 embedded in the nHKUST-1⊂MOF-5 sample is 11 wt %, consistent with the data obtained by the ^{1}H NMR analysis. Thermogravimetric data of nHKUST-1⊂MOF-5 were measured to determine thermal stability. Figure S2 in the Supporting Information indicates that nHKUST-1⊂MOF-5 is stable above 400 °C.

Both the bright- and the dark-field optical microscopic images of nHKUST-1⊂MOF-5 were compared to show the light-scattering from small particles inside the sample (Figure 4a). While the bright-field image in the inset of Figure 4a shows a clear and transparent cubic crystal, the dark-field image shows a glittering and multicolored crystal, which is attributed to the light-scattering of the HKUST-1 nanocrystals embedded in the MOF-5. Also, the SEM images of the crystal surface and the

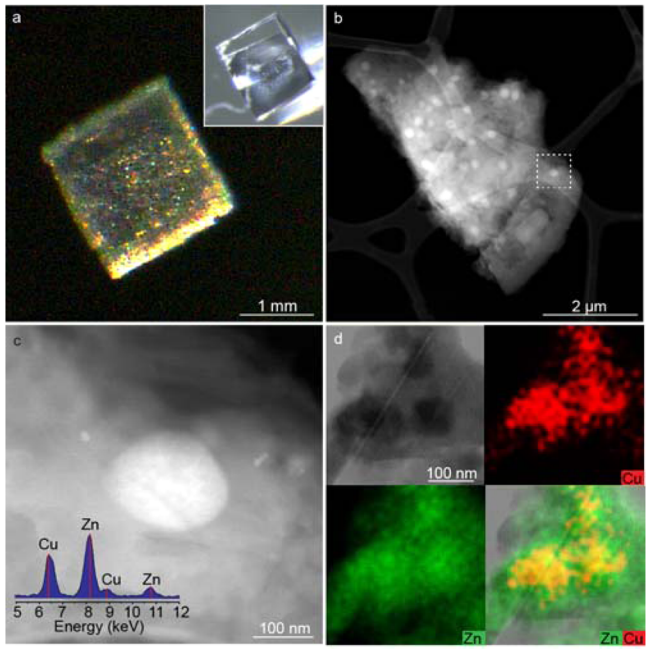

Figure 4. (a) Dark-field optical microscopic image of nHKUST-1⊂MOF-5, where the inset is an image obtained from a bright-field optical microscope. (b) HAADF STEM image of the broken piece of nHKUST-1⊂MOF-5. (c) HAADF STEM image under high magnification of the part marked in (b); the inset is an elemental analysis of nHKUST-1⊂MOF-5. (d) Elemental mapping of nHKUST-1⊂MOF-5.

DOI: 10.1021/acs.chemmater.5b01786
Chem. Mater. 2015, 27, 5088−5093

interior of nHKUST-1⊂MOF-5 demonstrate that nHKUST-1 particles were embedded in MOF-5 (Supporting Information Figure S3). The interior of nHKUST-1⊂MOF-5 exhibited nanocrystals (ca. 100 nm) of nHKUST-1, while its surface was smooth, similar to a typical MOF-5 crystal (Supporting Information Figure S3). These optical and electron microscopy images coupled with observations of PXRD and nitrogen gas-adsorption isotherm measurements provide evidence of nHKUST-1 crystals embedded in MOF-5, thus resulting in the formation of nHKUST-1⊂MOF-5.

Moreover, to provide further evidence of the embedment of nHKUST-1 particles in the MOF-5 crystals, the crystals of nHKUST-1⊂MOF-5 were broken into small pieces and analyzed by HAADF STEM. Figure 4b and the enlarged image of a local part in Figure 4b (Figure 4c) give clear evidence that the nHKUST-1 particles (ca. 100 nm) are embedded and well distributed in the MOF-5 matrix. In addition, an elemental analysis (EA) of the entire area in Figure 4c shows the existence of Cu (6.4 and 8.9 keV) from nHKUST-1 as well as Zn (8.2 and 10.8 keV) from MOF-5.[30,31] These findings clarify that the small particle shown in Figure 4b is an nHKUST-1 crystal embedded in MOF-5 (Figure 4c). Furthermore, the elemental mapping result shows the distribution of Cu from nHKUST-1 and that of Zn from MOF-5 (Figure 4d). We also observed the interface of nHKUST-1 and MOF-5 closely from two randomly selected spots on the nHKUST-1⊂MOF-5 sample (Supporting Information Figure S4). In the HRTEM images of the two spots (Supporting Information Figure S4a and c), the darker area in the middle is nHKUST-1 (100 nm in size) and the surrounding area is MOF-5. The enlarged image of Supporting Information Figure S4a is also shown in Supporting Information Figure S4b, while the HAADF STEM image in Supporting Information Figure S4c is shown in Supporting Information Figure S4d. As observed in all images in Supporting Information Figure S4, there are no spaces between the two different MOFs. This indicates that the compartments of MOF-5 and HKUST-1 are directly linked at their boundary, which creates the unusual interface that contributes to the enhanced gas uptake properties.

The ability to embed nanocrystals of one MOF into the crystals of another MOF would open many opportunities to create valuable applications. As an example to demonstrate this potential, we initially included molecular dyes in the pores of nHKUST-1 by adding rhodamine at an amount of 10^{-4} mol % to its synthesis solution. Given that the diameter of rhodamine, approximately 1 nm in size, is smaller than the pore size of 1.35 nm of nHKUST-1 and larger than its pore aperture of 0.6 nm,[12] we found that rhodamine molecules could be encapsulated inside the pores of nHKUST-1, as demonstrated by the UV measurements. The dye⊂nHKUST-1 crystal was then embedded in a MOF-5 crystal to form the (dye⊂nHKUST-1)⊂MOF-5 structure. In addition, confocal microscopy measurements were performed to show the existence as well as the distribution of the dyes in the MOF-5, dye⊂nHKUST-1, and (dye⊂nHKUST-1)⊂MOF-5 structures (Figure 5). The luminescence was not obtained from MOF-5 crystals (Figure 5a), while being obtained from dye⊂nHKUST-1 (Figure 5b). The (dye⊂nHKUST-1)⊂MOF-5 sample showed homogeneous luminescence throughout the crystals. These findings support that the dye⊂nHKUST-1 particles are successfully embedded and well distributed inside the MOF-5 crystals. In addition, these data for molecular inclusion are also evidence

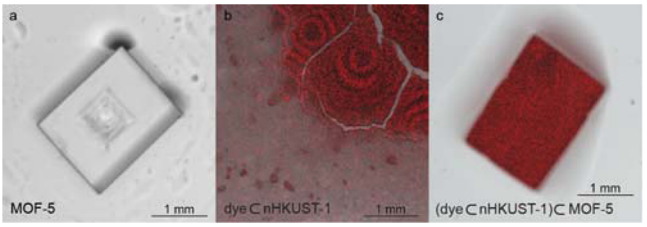

Figure 5. Image obtained using confocal microscopy measurements of the MOF-5, dye⊂nHKUST-1, and (dye⊂nHKUST-1) ⊂MOF-5 structures.

that the nHKUST-1 particles were embedded in the crystals of MOF-5.

nHKUST-1⊂MOF-5 showed a high uptake capacity as an energy-carrier of CH_4 at room temperature. The uptake capacity was measured with a magnetic suspension balance (MSB, Rubotherm). It was determined that the uptake capacity of CH_4 in nHKUST-1⊂MOF-5 was 197 mg/g, which was 14% and 36% higher than those of nHKUST-1 and MOF-5 at room temperature, respectively (Figure 6a). Also, the deliverable volumetric capacity of nHKUST-1⊂MOF-5 from 5.8 to 80 bar is 184 V_{STP}/V. When compared to a CNG tank,[32] this finding demonstrates that nHKUST-1⊂MOF-5 can deliver up to the 250% of the deliverable volumetric capacity of fuel delivered by a CNG tank at 80 bar. Moreover, Figure 6b shows that nHKUST-1⊂MOF-5 samples synthesized from different batches gave identical CH_4 uptake results. It is important to note that the experimentally tested error for a nonporous sample was within 0.0003 mg/g (Figure 6b). In addition, we tested the cyclic performance of CH_4 adsorption at room temperature, finding that nHKUST-1⊂MOF-5 shows robust performance for reversible cycles (Figure 6c). Moreover, the larger was the amount of nHKUST-1 embedded in MOF-5, the higher was the methane uptake (Supporting Information Figure S5). This implies that the combination of two different MOFs provides new interfaces that are responsible for enhancing the gas uptake capabilities. We speculate that new types of defects formed at the interface of the two MOFs can contribute to enhanced methane uptake capacity. These results support the claim that the embedded nanocrystals of one MOF into another MOF crystal can provide a new route to realize the performance required for advanced applications.

■ CONCLUSIONS

In summary, we developed a synthetic method for embedding the nanocrystals of one MOF into the crystals of another MOF with different structures and microspore moieties, where nHKUST-1 was synthesized to a size of about 100 nm and then embedded in the crystals of MOF-5. The crystal structures, porosities, the embedded constructs, and the chemical compositions were fully characterized. Moreover, as examples to explore the potential of the nHKUST-1⊂MOF-5 structure, we demonstrated guest dye molecules in nMOFs, which were then embedded into other MOF crystals. Furthermore, we showed that nHKUST-1⊂MOF-5 at room temperature and 80 bar has an enhanced gravimetric capacity for CH_4 uptake as compared to that of pristine HKUST-1 or MOF-5 alone, corresponding to 250% of the volumetric capacity for fuel storage deliverable of a commercial CNG tank. Robust capacity retention with no hysteresis was also noted.

DOI: 10.1021/acs.chemmater.5b01786
Chem. Mater. 2015, 27, 5088−5093

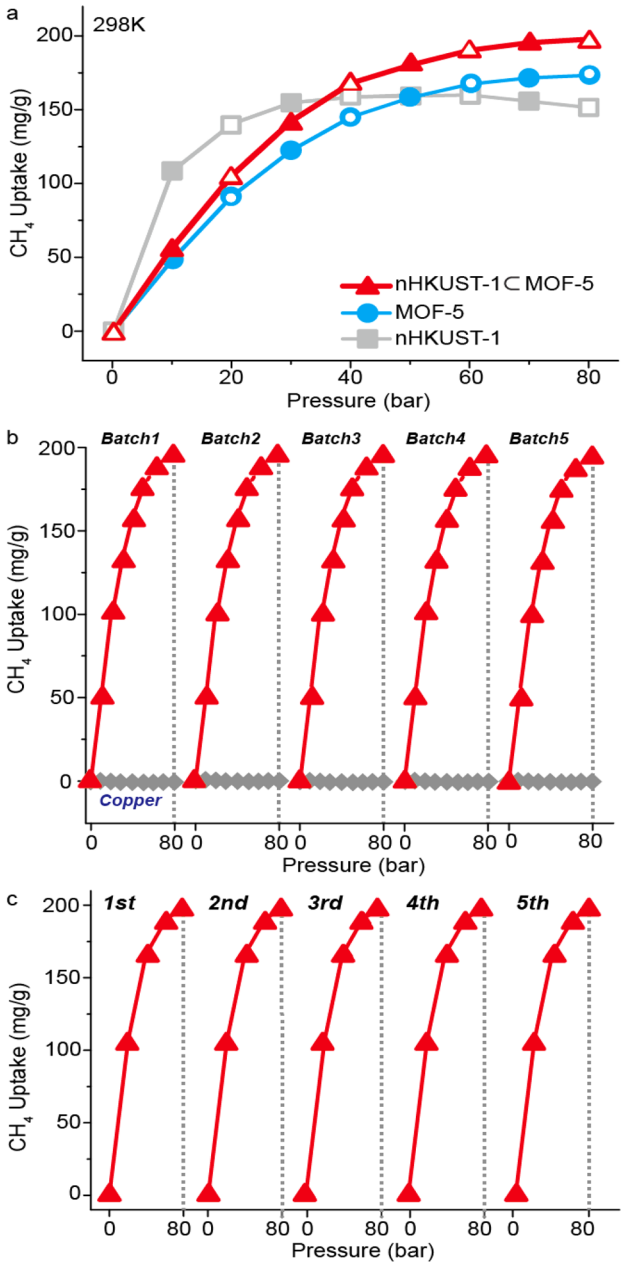

Figure 6. Adsorption performance for methane (CH_4) at room temperature: (a) the gravimetric adsorption uptake capacity of nHKUST-1⊂MOF-5, MOF-5, and nHKUST-1, (b) the adsorption performance with different batch experiments, and (c) the performance with regard to reversible adsorption cycles on nHKUST-1⊂MOF-5.

■ ASSOCIATED CONTENT

Supporting Information

Details of the materials characterization processes, the pore-size distribution, the thermogravimetric data, the images of SEM, HRTEM, and HAADF STEM, and the methane uptakes for nHKUST-1⊂MOF-5. The Supporting Information is available free of charge on the ACS Publications website at DOI: 10.1021/acs.chemmater.5b01786.

■ AUTHOR INFORMATION

Corresponding Author

*E-mail: jeung@kaist.ac.kr.

Author Contributions

†K.M.C. and J.H.P. contributed equally.

Notes

The authors declare no competing financial interest.

■ ACKNOWLEDGMENTS

This research was supported by the Global Frontier R&D Program of the Center for Hybrid Interface Materials (2013M3A6B1078884), by the Korea Center for Artificial Photosynthesis (2009-0093881), and by the National Research Foundation of Korea (2011-0028737 and 2012M1A2A2671813) funded by the Ministry of Science, ICT & Future Planning (MSIP). We especially thank Dong Ki Lee for the discussion about the TEM images and Prof. Omar Yaghi for the fruitful discussions about the synthesis of MOFs.

■ REFERENCES

(1) Chen, B. L.; Xiang, S. C.; Qian, G. D. Metal-Organic Frameworks with Functional Pores for Recognition of Small Molecules. *Acc. Chem. Res.* **2010**, *43*, 1115−1124.

(2) Deng, H. X.; Doonan, C. J.; Furukawa, H.; Ferreira, R. B.; Towne, J.; Knobler, C. B.; Wang, B.; Yaghi, O. M. Multiple Functional Groups of Varying Ratios in Metal-Organic Frameworks. *Science* **2010**, *327*, 846−850.

(3) Turner, S.; Lebedev, O. I.; Schroder, F.; Esken, D.; Fischer, R. A.; Van Tendeloo, G. Direct Imaging of Loaded Metal-Organic Framework Materials (Metal@MOF-5). *Chem. Mater.* **2008**, *20*, 5622−5627.

(4) Gu, X. J.; Lu, Z. H.; Jiang, H. L.; Akita, T.; Xu, Q. Synergistic Catalysis of Metal-Organic Framework-Immobilized Au-Pd Nanoparticles in Dehydrogenation of Formic Acid for Chemical Hydrogen Storage. *J. Am. Chem. Soc.* **2011**, *133*, 11822−11825.

(5) James, S. L. Metal-Organic Frameworks. *Chem. Soc. Rev.* **2003**, *32*, 276−288.

(6) Li, H.; Eddaoudi, M.; O'Keeffe, M.; Yaghi, O. M. Design and Synthesis of An Exceptionally Stable and Highly Porous Metal-Organic Framework. *Nature* **1999**, *402*, 276−279.

(7) Lee, J.; Farha, O. K.; Roberts, J.; Scheidt, K. A.; Nguyen, S. T.; Hupp, J. T. Metal-Organic Framework Materials as Catalysts. *Chem. Soc. Rev.* **2009**, *38*, 1450−1459.

(8) Wang, C.; Xie, Z. G.; deKrafft, K. E.; Lin, W. L. Doping Metal-Organic Frameworks for Water Oxidation, Carbon Dioxide Reduction, and Organic Photocatalysis. *J. Am. Chem. Soc.* **2011**, *133*, 13445−13454.

(9) Fu, Y. H.; Sun, D. R.; Chen, Y. J.; Huang, R. K.; Ding, Z. X.; Fu, X. Z.; Li, Z. H. An Amine-Functionalized Titanium Metal-Organic Framework Photocatalyst with Visible-Light-Induced Activity for CO2 Reduction. *Angew. Chem., Int. Ed.* **2012**, *51*, 3364−3367.

(10) Demessence, A.; D'Alessandro, D. M.; Foo, M. L.; Long, J. R. Strong CO_2 Binding in a Water-Stable, Triazolate-Bridged Metal-Organic Framework Functionalized with Ethylenediamine. *J. Am. Chem. Soc.* **2009**, *131*, 8784−8786.

(11) Kaye, S. S.; Dailly, A.; Yaghi, O. M.; Long, J. R. Impact of Preparation and Handling on the Hydrogen Storage Properties of Zn_4O(1,4-benzenedicarboxylate)$_3$ (MOF-5). *J. Am. Chem. Soc.* **2007**, *129*, 14176−14177.

(12) Chui, S. S. Y.; Lo, S. M. F.; Charmant, J. P. H.; Orpen, A. G.; Williams, I. D. A Chemically Functionalizable Nanoporous Material $[Cu_3(TMA)_2(H_2O)_3]_n$. *Science* **1999**, *283*, 1148−1150.

(13) Joo, S. H.; Park, J. Y.; Tsung, C.-K.; Yamada, Y.; Yang, P.; Somorjai, G. A. Thermally Stable Pt/mesoporous Silica Core-shell Nanocatalysts for High-temperature Reactions. *Nat. Mater.* **2009**, *8*, 126−131.

(14) Lim, D.-K.; Jeon, K.-S.; Hwang, J.-H.; Kim, H.; Kwon, S.; Suh, Y. D.; Nam, J.-M. Highly Uniform and Reproducible Surface-enhanced Raman Scattering from DNA-tailorable Nanoparticles with 1-nm Interior Gap. *Nat. Nanotechnol.* **2011**, *6*, 452−460.

DOI: 10.1021/acs.chemmater.5b01786
Chem. Mater. 2015, 27, 5088−5093

(15) Catala, L.; Brinzei, D.; Prado, Y.; Gloter, A.; Stephan, O.; Rogez, G.; Mallah, T. Core-Multishell Magnetic Coordination Nanoparticles: Toward Multifunctionality on the Nanoscale. *Angew. Chem., Int. Ed.* **2009**, *48*, 183−187.
(16) Dia, N.; Lisnard, L.; Prado, Y.; Gloter, A.; Stephan, O.; Brisset, F.; Hafez, H.; Saad, Z.; Mathoniere, C.; Catala, L.; Mallah, T. Synergy in Photomagnetic/Ferromagnetic Sub-50 nm Core-Multishell Nanoparticles. *Inorg. Chem.* **2013**, *52*, 10264−10274.
(17) Zheng, P.; Jiang, X.; Zhang, X.; Zhang, W.; Shi, L. Formation of Gold@Polymer Core-shell Particles and Gold Particle Clusters on a Template of Thermoresponsive and pH-responsive Coordination Triblock Copolymer. *Langmuir* **2006**, *22*, 9393−9396.
(18) Wang, C.; Chi, M.; Wang, G.; van der Vliet, D.; Li, D.; More, K.; Wang, H.-H.; Schlueter, J. A.; Markovic, N. M.; Stamenkovic, V. R. Correlation Between Surface Chemistry and Electrocatalytic Properties of Monodisperse Pt_xNi_{1-x} Nanoparticles. *Adv. Funct. Mater.* **2011**, *21*, 147−152.
(19) Zhang, S.; Metin, O.; Su, D.; Sun, S. Monodisperse AgPd Alloy Nanoparticles and Their Superior Catalysis for the Dehydrogenation of Formic Acid. *Angew. Chem., Int. Ed.* **2013**, *52*, 3681−3684.
(20) Zhou, S. H.; Varughese, B.; Eichhorn, B.; Jackson, G.; McIlwrath, K. Pt-Cu Core-shell and Alloy Nanoparticles for Heterogeneous NO_x, Reduction: Anomalous Stability and Reactivity of a Core-shell nanostructure. *Angew. Chem., Int. Ed.* **2005**, *44*, 4539−4543.
(21) Cui, C.; Gan, L.; Heggen, M.; Rudi, S.; Strasser, P. Compositional Segregation in Shaped Pt Alloy Nanoparticles and Their Structural Behaviour During Electrocatalysis. *Nat. Mater.* **2013**, *12*, 765−771.
(22) He, L.; Liu, Y.; Liu, J.; Xiong, Y.; Zheng, J.; Liu, Y.; Tang, Z. Core-Shell Noble-Metal@Metal-Organic-Framework Nanoparticles with Highly Selective Sensing Property. *Angew. Chem., Int. Ed.* **2013**, *52*, 3741−3745.
(23) Jiang, H.-L.; Liu, B.; Akita, T.; Haruta, M.; Sakurai, H.; Xu, Q. Au@ZIF-8: CO Oxidation over Gold Nanoparticles Deposited to Metal-Organic Framework. *J. Am. Chem. Soc.* **2009**, *131*, 11302−11303.
(24) Ke, F.; Qiu, L.-G.; Yuan, Y.-P.; Jiang, X.; Zhu, J.-F. Fe_3O_4@MOF Core-shell Magnetic Microspheres with a Designable Metal-Organic Framework Shell. *J. Mater. Chem.* **2012**, *22*, 9497−9500.
(25) Ke, F.; Wang, L.; Zhu, J. Multifunctional Au-Fe_3O_4@MOF Core-shell Nanocomposite Catalysts with Controllable Reactivity and Magnetic Recyclability. *Nanoscale* **2015**, *7*, 1201−1208.
(26) Lu, G.; Li, S.; Guo, Z.; Farha, O. K.; Hauser, B. G.; Qi, X.; Wang, Y.; Wang, X.; Han, S.; Liu, X.; DuChene, J. S.; Zhang, H.; Zhang, Q.; Chen, X.; Ma, J.; Loo, S. C. J.; Wei, W. D.; Yang, Y.; Hupp, J. T.; Huo, F. Imparting Functionality to a Metal-Organic Framework Material by Controlled Nanoparticle Encapsulation. *Nat. Chem.* **2012**, *4*, 310−316.
(27) Na, K.; Choi, K. M.; Yaghi, O. M.; Somorjai, G. A. Metal Nanocrystals Embedded in Single Nanocrystals of MOFs Give Unusual Selectivity as Heterogeneous Catalysts. *Nano Lett.* **2014**, *14*, 5979−5983.
(28) Koh, K.; Wong-Foy, A. G.; Matzger, A. J. MOF@MOF: Microporous Core-shell Architectures. *Chem. Commun.* **2009**, 6162−6164.
(29) Li, T.; Sullivan, J. E.; Rosi, N. L. Design and Preparation of a Core-Shell Metal-Organic Framework for Selective CO_2 Capture. *J. Am. Chem. Soc.* **2013**, *135*, 9984−9987.
(30) Zuo, L.; Chen, S. H.; Wu, J. F.; Wang, L.; Hou, H. Q.; Song, Y. H. Facile Synthesis of Three-Dimensional Porous Carbon with High Surface Area by Calcining Metal-Organic Framework for Lithium-on Batteries Anode Materials. *RSC Adv.* **2014**, *4*, 61604−61610.
(31) Zhang, N. T.; Zhu, B. J.; Peng, F. M.; Yu, X. Y.; Jia, Y.; Wang, J.; Kong, L. T.; Jin, Z.; Luo, T.; Liu, J. H. Synthesis of Metal-Organic-Framework related Core-shell Heterostructures and Their Application to Ion Enrichment in Aqueous Conditions. *Chem. Commun.* **2014**, *50*, 7686−7689.
(32) Wilmer, C. E.; Farha, O. K.; Yildirim, T.; Eryazici, I.; Krungleviciute, V.; Sarjeant, A. A.; Snurr, R. Q.; Hupp, J. T. Gram-scale, High-yield Synthesis of a Robust Metal-Organic Framework for Storing Methane and Other Gases. *Energy Environ. Sci.* **2013**, *6*, 1158−1163.

DOI: 10.1021/acs.chemmater.5b01786
Chem. Mater. 2015, 27, 5088−5093